Structures of the *Escherichia coli* PutA Proline Dehydrogenase Domain in Complex with Competitive Inhibitors[†,‡]

Min Zhang,[§] Tommi A. White,[§] Jonathan P. Schuermann,[§] Berevan A. Baban,[||,⊥] Donald F. Becker,[||] and John J. Tanner*[,§]

Departments of Chemistry and Biochemistry, University of Missouri−Columbia, Columbia, Missouri 65211, and Department of Biochemistry, Redox Biology Center, University of Nebraska, Lincoln, Nebraska 68588

Received June 17, 2004; Revised Manuscript Received July 29, 2004

ABSTRACT: Proline dehydrogenase (PRODH) catalyzes the first step of proline catabolism, the flavin-dependent oxidation of proline to Δ^1-pyrroline-5-carboxylate. Here we present a structure-based study of the PRODH active site of the multifunctional *Escherichia coli* proline utilization A (PutA) protein using X-ray crystallography, enzyme kinetic measurements, and site-directed mutagenesis. Structures of the PutA PRODH domain complexed with competitive inhibitors acetate (K_i = 30 mM), L-lactate (K_i = 1 mM), and L-tetrahydro-2-furoic acid (L-THFA, K_i = 0.2 mM) have been determined to high-resolution limits of 2.1−2.0 Å. The discovery of acetate as a competitive inhibitor suggests that the carboxyl is the minimum functional group recognized by the active site, and the structures show how the enzyme exploits hydrogen-bonding and nonpolar interactions to optimize affinity for the substrate. The PRODH/L-THFA complex is the first structure of PRODH with a five-membered ring proline analogue bound in the active site and thus provides new insights into substrate recognition and the catalytic mechanism. The ring of L-THFA is nearly parallel to the middle ring of the FAD isoalloxazine, with the inhibitor C5 atom 3.3 Å from the FAD N5. This geometry suggests direct hydride transfer as a plausible mechanism. Mutation of conserved active site residue Leu432 to Pro caused a 5-fold decrease in k_{cat} and a severe loss in thermostability. These changes are consistent with the location of Leu432 in the hydrophobic core near residues that directly contact FAD. Our results suggest that the molecular basis for increased plasma proline levels in schizophrenic subjects carrying the missense mutation L441P is due to decreased stability of human PRODH2.

Proline has a central role in metabolism and can serve as an important energy source (*1*, *2*). All organisms recycle proline by oxidizing it to glutamate in two enzymatic steps. In the first step, proline is oxidized to Δ^1-pyrroline-5-carboxylate (P5C)[1] by the flavoenzyme proline dehydrogenase (PRODH, Figure 1). P5C is hydrolyzed nonenzymatically to glutamic semialdehyde, and the semialdehyde is oxidized to glutamate by the NAD-dependent enzyme P5C dehydrogenase (P5CDH). The collective activities of PRODH and P5CDH result in the 4-electron oxidation of proline to glutamate. The glutamate produced by proline catabolism readily enters the TCA cycle as α-ketoglutarate, following oxidative deamination by glutamate dehydrogenase. Alternatively, several enzymatic steps transform glutamate into acetyl-CoA, which enters the TCA cycle for energy metabolism, generating ATP.

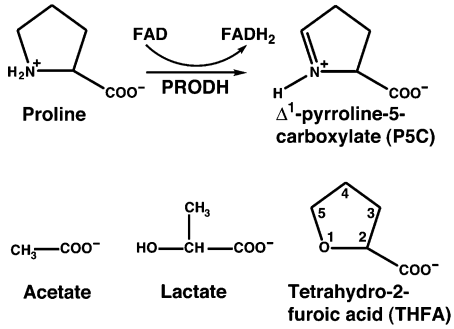

FIGURE 1: The reaction catalyzed by the PutA proline dehydrogenase domain (top) and chemical structures of the three inhibitors used in this study (bottom).

In eukaryotes, PRODH and P5CDH are distinct enzymes that are encoded by two separate genes (*1*). Humans have two isozymes of PRODH. A protein encoded on chromosome 19 has been named PRODH1, and a second protein identified as PRODH2 is encoded on chromosome 22. PRODH1 is predicted to express almost exclusively in the liver and kidney while PRODH2 expression is predicted in the brain, heart, pancreas, kidney, and liver. PRODH2 has received

[†] This work was supported by NIH Grants GM065546 (to J.J.T.) and GM061068 (to D.F.B.) and the Nebraska Agricultural Research Division, Journal Series No. 14681.

[‡] Coordinates and structure factors have been deposited in the Protein Data Bank under Accession Numbers 1TJ1, 1TJ2, 1TJ0, and 1TIW.

* Address correspondence to this author. Tel: 573-884-1280. Fax: 573-882-2754. E-mail: tannerjj@missouri.edu.

[§] University of Missouri−Columbia.

[||] University of Nebraska.

[⊥] Present address: Department of Anatomy and Neurobiology, Washington University School of Medicine, 660 South Euclid Ave., Campus Box 8108, St. Louis, MO 63110.

[1] Abbreviations: PutA, proline utilization A; FAD, flavin adenine dinucleotide; PRODH, proline dehydrogenase; P5C, Δ^1-pyrroline-5-carboxylate; P5CDH, Δ^1-pyrroline-5-carboxylate dehydrogenase; THFA, tetrahydro-2-furoic acid; RMSD, root mean square deviation; MTHFR, methylenetetrahydrofolate reductase.

10.1021/bi048737e CCC: $27.50 © 2004 American Chemical Society
Published on Web 09/04/2004

attention due to its involvement in human health and disease, including reactive oxygen species generation in cancer cell lines, control of cellular redox status, and p53-induced apopotosis (*3*−*5*). Also, the *PRODH2* gene has been proposed as a possible schizophrenia susceptibility gene on the basis of genetic linkage analysis (*6*−*8*), although this association is a subject of debate (*9*−*11*).

The PRODH and P5CDH activities in most bacteria are combined into the single polypeptide of the PutA (proline utilization A) flavoprotein (*12*−*17*). PutA proteins are peripheral membrane-associated enzymes (*12*, *18*) that typically consist of 1000−1300 amino acid residues, with the PRODH domain invariably located in the N-terminal half of the polypeptide chain and the P5CDH domain in the C-terminal half. In addition to the PRODH and P5CDH activities, some PutA proteins serve as repressors of their own gene, with the *Escherichia coli* and *Salmonella typhimurium* proteins being archetypal examples (*14*, *19*−*21*). *E. coli* PutA consists of 1320 residues and is believed to function as a homodimer. Amino acid sequence alignments readily show that the PRODH and P5CDH domains are located within residues 228−572 and 656−1106, respectively. The DNA-binding domain was recently identified as residues 1−47, using a combination of molecular dissection and sequence analysis (*22*). The location of the membrane-binding domain is currently an open question.

Inhibition of eukaryotic PRODH and bacterial PutA by Pro analogues has been studied to understand the catalytic mechanism and the relationship between proline degradation and metabolic pathways such as glycolysis. Also, PRODH inhibitors have been sought to control the tsetse fly, a transmitter of the protozoan parasite *Trypanosoma brucei*, which causes African sleeping sickness (*23*). L-Lactate is a competitive inhibitor of both eukaryotic PRODH (*24*) and *E. coli* PutA (K_i = 1.4 mM) (*25*). Inhibition of *E. coli* PutA by L-tetrahydro-2-furoic acid (L-THFA) was investigated previously (*26*). This inhibitor is especially interesting because it is isostructural with the substrate proline (Figure 1). L-THFA displays simple competitive inhibition of PRODH activity with an apparent K_i of 0.2 mM. Binding of L-THFA perturbs the FAD absorbance spectrum and changes the redox potential by −12 mV. Whereas L-lactate and L-THFA are reversible inhibitors, 4-methylene-L-proline is oxidized by PRODH to an electrophilic species which is thought to react with a nucleophilic group in the active site (*23*).

We recently determined the crystal structure of the PRODH domain of *E. coli* PutA, which was the first structure of a PRODH enzyme from any organism (*27*). Here we present an analysis of the *E. coli* PutA PRODH active site using crystallography, enzyme kinetic measurements, and site-directed mutagenesis. Structures of the PRODH domain complexed with competitive inhibitors acetate, L-lactate, and L-THFA provide insights into catalytic mechanism, substrate recognition, and the roles of active site residues. Analysis of these structures shows that the PRODH active site shares several features in common with other flavin-dependent dehydrogenases. Mutation of conserved residue Leu432 to Pro results in a loss of activity and thermostability, which is consistent with the location of Leu432 near the FAD cofactor, and the participation of the Leu side chain in the hydrophobic core.

MATERIALS AND METHODS

Subcloning of the PutA86−*669 Construct.* The design plan for PutA86−669 was based on previous experience with a construct known as PutA669, which corresponds to residues 1−669 of full-length *E. coli* PutA (*28*). Whereas crystals of PutA669 led to the first structure of a PRODH domain, these crystals were very difficult to reproduce due to proteolytic degradation of PutA669, and thus an improved construct was sought for the present studies. Gel electrophoresis of PutA669 crystals clearly indicated a protein much smaller than the expected molecular mass of 76 kDa. MALDI-TOF mass spectroscopy of PutA669 crystals performed by the University of Missouri−Columbia Proteomics Center returned an unambiguous result of 61 kDa. Consideration of the (1) amino acid sequence, (2) mass spectral data, and (3) knowledge of which residues had been resolved in the PutA669 structure suggested proteolysis had occurred at two sites, residue 82 ± 5 and residue 632 ± 5. Thus, constructs corresponding to *E. coli* PutA residues 86−669 (PutA86−669) and 86−630 (PutA86−630; not described here) were engineered.

PutA86−669 was prepared in pUTA669 [a pET-23b construct encoding residues 1−669 of PutA with a C-terminal hexahistidine tag (*29*)] using QuikChange (Stratagene) site-directed mutagenesis. An *Nde*I site was introduced at amino acid codon 84 of the *putA* gene in pUTA669. *Nde*I digestion of the modified *putA* gene resulted in PutA86−669. The cloning ends of the PutA86−669 construct were confirmed by nucleic acid sequencing.

Mutagenesis and Enzyme Assays. The L432P mutation was introduced into PutA86−669 using QuikChange, and the mutation was verified by sequencing. PRODH activity was measured using the proline−dichlorophenolindophenol oxidoreductase activity assay as described previously for PutA proteins (*12*, *13*, *28*, *30*). One unit of PRODH activity is the quantity of enzyme that transfers electrons from 1 μmol of proline to dichlorophenolindophenol per minute at 25 °C. Kinetic parameters for wild-type and mutant PutA86−669 were obtained from Lineweaver−Burk analysis using proline as the variable substrate in the range 0.025−0.4 M at fixed [FAD] = 17.5 μM. Each measurement was performed three times, and the average values were input to linear regression analysis to estimate kinetic constants.

Inhibition by acetate was examined by steady-state inhibition kinetic measurements using proline as the variable substrate ([Pro] = 0.025−0.4 M, [FAD] = 17.5 μM) at fixed sodium acetate concentrations of 0, 0.05, 0.1, and 0.2 M. The pH of the 3 M sodium acetate stock solution used for these studies was adjusted with HCl to match the pH of the reaction buffer to ensure that no change in pH occurred upon addition of the inhibitor.

Thermostability was estimated by measuring PRODH activity as a function of time at 45 °C. A sample of protein was incubated at 45 °C, and aliquots were removed at various time points and stored at 4 °C. After all of the aliquots were taken and cooled to 4 °C, activity assays were conducted at 25 °C in the presence of 0.4 M proline and 17.5 μM FAD.

Purification and Crystallization. Wild-type PutA86−669 was overexpressed in *E. coli* strain BL21(DE3) pLysS and purified with Ni-NTA affinity (Qiagen) and anion-exchange (HiTrapQ, Pharmacia) chromatography using procedures

Table 1: Data Collection and Refinement Statistics[a]

	crystal form			
	I	II	III	IV
bound inhibitor	L-lactate	acetate	L-lactate	L-THFA
inhibitor concn (mM)	0	0	10	10
precipitating agent	PEG 3000	PEG 3350	PEG 3350	PEG 3350
PDB accession code	1TJ1	1TJ2	1TJ0	1TIW
wavelength (Å)	0.979338	0.97856	0.97856	0.97856
space group	*I*222	*I*222	*I*222	*I*222
unit cell dimensions (Å)				
a	72.8	72.9	72.2	72.6
b	141.1	141.1	139.4	141.4
c	146.0	145.4	146.1	145.9
diffraction resolution (Å)	40−2.00	23−2.05	25−2.10	25−2.00
outer shell (Å)	2.06−2.00	2.11−2.05	2.16−2.10	2.06−2.00
no. of observations	293881	310065	291480	396042
no. of unique reflections	50059	45470	42999	50385
redundancy	5.9 (4.4)	6.8 (5.4)	6.8 (5.4)	7.9 (6.7)
completeness (%)	98 (91)	97 (91)	99 (92)	99 (91)
mean I/σ_I	23 (2.1)	14 (2.9)	24 (2.8)	25 (4.2)
R_{merge}	0.076 (0.469)	0.084 (0.405)	0.072 (0.485)	0.068 (0.352)
no. of protein residues	450	450	469	459
no. of protein atoms	3474	3477	3605	3545
no. of water molecules	194	193	198	195
R_{cryst}	0.214 (0.311)	0.208 (0.253)	0.212 (0.271)	0.214 (0.270)
R_{free}[b]	0.255 (0.366)	0.250 (0.311)	0.259 (0.358)	0.253 (0.292)
coordinate error (Å)	0.14	0.15	0.17	0.14
RMSD bond lengths (Å)[c]	0.014	0.014	0.015	0.014
RMSD bond angles (deg)[c]	1.4	1.4	1.4	1.4
Ramachandran plot[d]				
favored (no. of residues)	370	369	382	377
allowed (no. of residues)	23	24	27	22
generous (no. of residues)	0	0	3	1
disallowed (no. of residues)	0	0	0	0
average *B*-factors (Å^2)				
protein	31	29	29	27
FAD	28	25	25	25
inhibitor	29	30	27	25
water	43	40	39	40

[a] Values for the outer resolution shell of data are given in parentheses. [b] 5% R_{free} test set. [c] Compared to the Engh and Huber force field (*48*). [d] The Ramachandran plot was generated with PROCHECK and includes only non-Gly and non-Pro residues (*49*).

similar to those previously described for PutA669 (*29*). One important difference from the PutA669 protocol was that PutA86−669 appeared in the flow-through of the anion-exchange step rather than in the elution gradient. Following the chromatography steps, FAD was added to a concentration of 0.1 mM, and the protein was dialyzed into 50 mM Tris-HCl, 1 mM EDTA, 50 mM NaCl, and 5% glycerol, pH 7.5. The sample was concentrated to a volume of 2 mL using a Millipore Ultrafree-15 centrifugal filter (50 kDa cutoff) and then desalted to remove excess FAD. The sample was concentrated a second time to a final concentration of 20 mg/mL. The protein concentration was determined using the BCA method (Pierce). The hexahistidine tag remained after purification. The molecular mass of the purified protein was determined by mass spectroscopy to be 66.8 kDa, which is close to the predicted molecular mass of 66.5 kDa.

L432P was expressed and purified using protocols similar to those described for the wild-type enzyme. The mutant, however, was not nearly as soluble or stable as the wild-type enzyme, which resulted in significantly lower yields.

PutA86−669 crystallized under the same conditions and in the same unit cell as the cleaved PutA669 protein, but the PutA86−669 crystals were highly reproducible. All crystallization experiments were performed at 295 K using the sitting-drop method of vapor diffusion with drops formed by mixing 5 μL of the reservoir and 5 μL of the protein solution (10−15 mg/mL). The reservoir solutions consisted of 13−15% PEG 3000 or PEG 3350 and 60−190 mM citrate buffer, pH 5.7. Yellow crystals typically appeared within 5 days and grew to a maximum dimension of 0.4 mm in 3 weeks. Attempts to crystallize L432P were unsuccessful.

Four crystal structures are presented here, corresponding to complexes with L-lactate (forms I and III), acetate (form II), and L-THFA (form IV). Form I crystals were grown in PEG 3000 without an inhibitor added to the protein prior to crystallization (Table 1), which resulted in L-lactate bound in the active site due to L-lactate contamination in PEG 3000 (*31*). Crystal form II was grown in PEG 3350 without an inhibitor added to the protein prior to crystallization (Table 1). This form has an acetate ion bound in the active site, which presumably derives from PEG 3350. To obtain the L-lactate and L-THFA complexes grown in PEG 3350 (forms III and IV), the appropriate inhibitor was added to the protein prior to crystallization (10 mM). Crystals were cryoprotected by replacing the mother liquor with cryobuffer (24% PEG 3350, 15% PEG 200, 0.1 M citrate buffer, pH 5.7). After being soaked a few minutes in the cryobuffer, the crystals were picked up with Hampton mounting loops and plunged into liquid nitrogen.

Data Collection, Model Building, and Refinement. The four structures were solved from data collected from four crystals at beamline 19-ID of the Structural Biology Center

at the Advanced Photon Source. The data were processed with HKL2000 (*32*). The crystals grew in space group *I*222 with one molecule per asymmetric unit, 58% solvent content, and a Matthews coefficient of 2.9 (*33*). The unit cell dimensions of the four crystal forms were similar and in the range $a = 72-73$ Å, $b = 139-141$ Å, and $c = 145-146$ Å. Structure refinement was performed with CNS (*34*) and REFMAC5 (*35*, *36*). The initial model for refinement was obtained from the previously solved *E. coli* PutA PRODH domain structure (PDB code 1K87). A common set of test reflections (5%) was used for all four refinements, and this set corresponded to the one used for refinement of PutA669. Model building was done with O. Topology and parameter files for FAD and inhibitors were created using the PRODRG server (*37*). Simulated annealing omit maps were calculated using CNS by omitting the inhibitor and residues within 3.9 Å of the inhibitor. Structure analysis was performed with PyMol (*38*), CNS, and the LPC server (*39*). See Table 1 for data collection and refinement statistics.

The electron density was quite strong and unambiguous for residues 88−144, 162−184, and 244−610 in all four of the PutA86−669 structures. Crystal form III provided the most complete tracing; residues 88−187 and 242−610 could be modeled with confidence. Similar interruptions in the main chain trace were observed in the PutA669 structure (PDB code 1K87). Although residues 611−669 were not observed in any of the structures, the protein had not been degraded by proteolysis. Mass spectroscopy of a PutA86−669 crystal returned an unambiguous result of 66.8 kDa. Thus, residues 611−669 appear to be disordered in the PutA86−669 structures.

The PutA669 model (1K87) included two additional helices (residues 209−215, 224−236) that have been omitted from the present structures. Electron density representing these helices was present in PutA86−669 maps; however, attempts to model these residues resulted in *B*-values greater than 100 Å^2, and thus these residues were omitted in the current models.

RESULTS

Overall Structure and Comparison to MTHFR. The central structural feature of PutA86−669 is a $\beta_8\alpha_8$ barrel (TIM barrel) formed by residues 263−561 with the FAD cofactor bound at the carboxyl termini of the strands of the barrel (Figure 2). Residues 88−140 form a three-helix arm that packs tightly against one side of the barrel. Residues 562−610 fold into three helices that also pack against the barrel, atop the three-helix arm.

Residues 141−187 belong to a structural domain that is poorly resolved in the PutA86−669 structures and in the previous PutA669 structure. Because residues 188−241 were not visible in the electron density, there was more than one crystallographically equivalent way to connect residue 187 to residue 242 in order to construct the PutA86−669 monomer. The interpretation shown in Figure 2 is a relatively compact monomer owing to the tight packing of the three-helix arm against the barrel. An alternative interpretation was proposed previously based on the PutA669 crystallographic data, in which the three-helix arm wraps around the $\beta_8\alpha_8$ barrel of a symmetry-related molecule, resulting in a highly extended monomer that forms an intimate domain-swapped dimer (*27*). The two interpretations are equivalent (they correspond to different choices of the asymmetric unit) and yield identical crystallographic refinement statistics. However, the compact monomer interpretation (Figure 2) seems appropriate for PutA86−669 based on recent evidence implicating residues 1−85 in dimerization of full-length PutA (*22*, *40*). Indeed, PutA86−669 lacks residues 1−85, and it purifies as an apparent monomer in Superdex 200 gel filtration chromatography (data not shown).

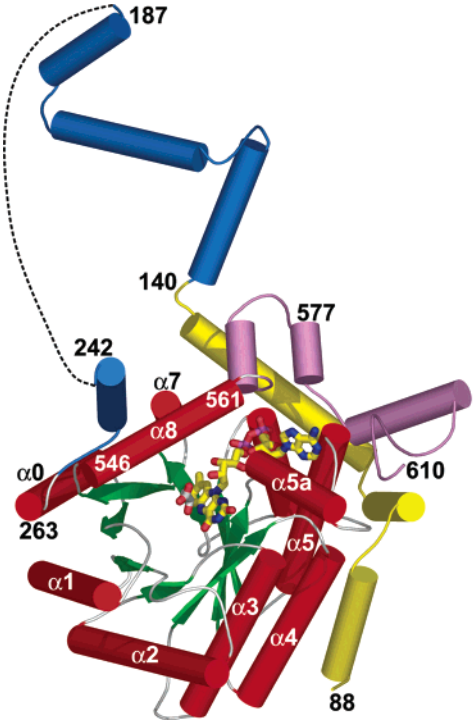

FIGURE 2: Ribbon drawing of PutA86−669 with bound L-lactate. The β/α barrel substructure is shown in green/red (residues 263−561). Helices of the barrel are labeled α0−α8, and selected residue numbers are indicated. Yellow cylinders indicate the helical arm that wraps around the barrel. Blue cylinders denote helices of a poorly resolved structural domain consisting of residues 141−262. The dashed curve indicates disordered residues. Purple cylinders denote helices positioned after the barrel. FAD and L-lactate are drawn as ball-and-stick models in yellow and white, respectively. This figure and others were prepared with PyMol (*38*).

Such tracing ambiguities are not uncommon, especially for crystals grown from engineered protein constructs corresponding to domains of large multidomain proteins. For example, a similar uncertainty in the main chain trace occurred in the structure of the cAMP-binding domain of Epac2 (*41*). In full-length PutA, residues 188−241 are probably stabilized by interactions with a domain not present in the PutA86−669 construct, and in the absence of these contacts, residues 188−241 are not properly folded. Despite the disordered residues, the PutA86−669 structures provide insights into the PRODH function because the electron density throughout the entire $\beta_8\alpha_8$ barrel is excellent.

The TIM barrel is a common fold for FMN-dependent enzymes, but it is uncommon for FAD-dependent enzymes. According to the SCOP database (*42*), there are 12 FMN-linked enzymes having the TIM barrel fold represented in the PDB, corresponding to 67 structures. In contrast, there are only two known examples of FAD cofactors bound to a TIM barrel, the PutA PRODH domain and methylenetetrahydrofolate reductase [MTHFR, PDB codes 1B5T (*43*) and 1V93].

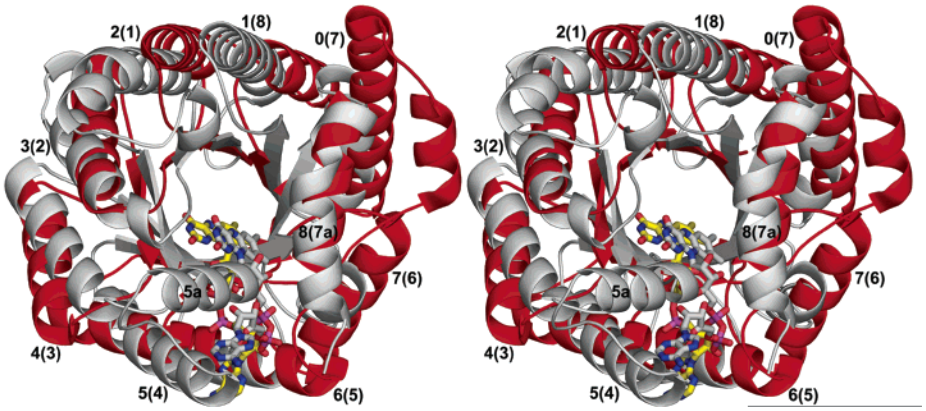

FIGURE 3: Stereoscopic view depicting the superposition of the β/α barrels of PutA86−669 (white) and methylenetetrahydrofolate reductase (red, PDB code 1B5T) (*43*). The FAD cofactor of PutA86−669 and methylenetetrahydrofolate reductase are shown in white and yellow, respectively. The helices of PutA are numbered 0−8, with the corresponding helices in MTHFR appearing in parentheses. This alignment was calculated using the CE server (*50*). The RMSD between the barrels of PutA and 1B5T is 3.4 Å for 188 aligned residues.

The PutA PRODH barrel exhibits three deviations from the classic $\beta_8\alpha_8$ topology. First, the barrel begins with a helix (α0) rather than a strand (Figure 2). This feature is also present, for example, in a yeast hypothetical protein (PDB code 1B54), which was identified as the top structural homologue of the PutA86−669 barrel by SSM (*44*). Second, there is a helix inserted between β5 and α5 (denoted α5a). This helix is functionally important because active site residues Tyr437 and Trp438 are located at its N-terminus. Finally, α8 is located above the barrel rather than alongside of it. The location of α8 is also critical for function because this helix contributes four active site residues, Tyr552, Arg555, Arg556, and Glu559. These residues are conserved among bacterial PutA proteins and eukaryotic PRODHs. Thus, α8 is critical for PutA's PRODH function.

While the PutA PRODH domain and MTHFR share a common fold, the two structures actually represent two distinct families of FAD-linked TIM barrel proteins. The two structures are related by a circular permutation of the barrel such that strands 1−8 of the PutA barrel correspond to strands 8,1−7 of the MTHFR barrel, and α0 of PutA aligns with α7 of MTHFR (Figure 3). Note that α8 of PutA aligns with α7a of MTHFR (residues 216−228). Helix α8 plays essential roles in PutA's PRODH function, as mentioned above. In contrast, α7a of MTHFR is a region of little sequence conservation and does not participate directly in binding substrates or cofactors (*43*). Thus, the interesting structural similarity, a deviation from the classic TIM barrel fold, does not extend to function in this case. Note also that the functionally important helix α5a of PutA does not have a counterpart in MTHFR.

FAD Binding Site. The FAD cofactor binds at the carboxyl termini of the strands of the barrel, with the dimethylbenzene edge pointing to β7 and the carbonyl edge pointing to β3 (Figure 2). The *re* face packs tightly against β4−6, while the *si* face is available for hydride transfer. This arrangement is similar to that seen in MTHFR, after accounting for the circular permutation of the barrel. That is, in MTHFR, the dimethyl and carbonyl edges point toward β6 and β2, respectively, and the *re* face is supported by β3−5 (Figure 3).

The FAD interacts with 35 residues through electrostatic (cutoff = 3.3 Å) and nonpolar (cutoff = 3.9 Å) interactions. Some of these interactions are depicted in a schematic diagram (Figure 4). The adenine stacks against Trp438 and hydrogen bonds to Thr457 and Thr462. The ribose hydrogen bonds to Gly435. The FAD in PutA is somewhat folded up such that a ribose hydroxyl hydrogen bonds to the ribityl 4′-hydroxyl. In contrast, the FAD in MTHFR is more extended, and no such intramolecular hydrogen bonding occurs. The pyrophosphate ion pairs to Lys434 and Lys459, and it hydrogen bonds to Thr486, His487, Asn488, and

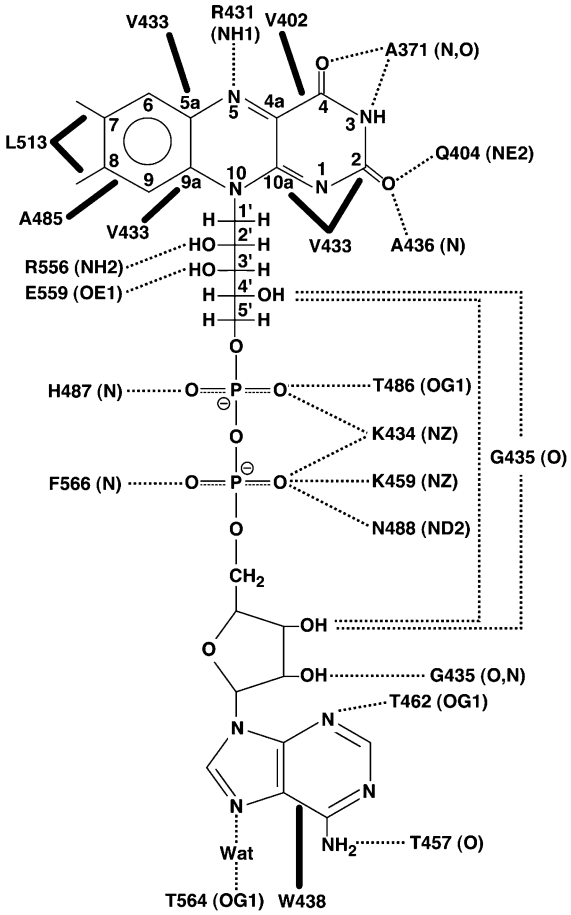

FIGURE 4: Schematic diagram of selected protein−FAD interactions. The dotted lines indicate hydrogen bonds and ion pairs, with the interacting atoms listed in parentheses. The thick solid lines indicate nonpolar interactions. Note that there is also an intramolecular hydrogen bond indicated, between the FAD ribose and ribityl groups.

Phe566. The 2′, 3′, and 4′ ribityl hydroxyls hydrogen bond to Arg556, Glu559, and Gly435, respectively.

The isoalloxazine is the hydride acceptor of FAD, and it forms several interactions with the protein. These interactions are presumably important for orienting the FAD for catalysis and for maintaining a redox potential of approximately −91 mV for the 2-electron reduction of the flavin (*28*). Arg431 donates a hydrogen bond to FAD N5, which is the hydride acceptor of the FAD. The pyrimidine ring of FAD hydrogen bonds to Ala371, Ala436, and Gln404. Finally, the *re* face is supported by nonpolar contacts with Val402, Val433, and Ala485, while the *si* face of the dimethylbenzene contacts Leu513.

Consistent with the many protein−FAD interactions listed above, the FAD is almost completely buried in the protein. The accessible surface area (ASA) of the protein-bound FAD in the THFA complex (crystal form IV) is only 28 Å^2, with the flavin N5 atom exposing 0 Å^2. For reference, the ASA of FAD separated from the protein is 938 Å^2. Thus, catalysis occurs in a solvent-protected environment, which is common for flavoenzyme dehydrogenases (*45*).

Inhibitor Binding Site. An L-lactate molecule was modeled into the active site of PutA669, based on a strong electron density feature located on the *si* side of the FAD isoalloxazine (*27*). An identical feature was observed in electron density maps for crystal form I of PutA86−669 (Figure 5A). We recently showed that the PEG 3000 solutions used for crystallization and cryoprotection of PutA669 and PutA86−669 contain millimolar levels of L-lactate (*31*), which explained the unexpected appearance of this inhibitor in the active site. Our study also showed that commercially available PEG 3350 is free of L-lactate contamination, and therefore PutA86−669 was crystallized in PEG 3350 (crystal form II) in order to determine the structure of the uninhibited enzyme. As a positive control, PutA86−669 was also crystallized in the presence of 10 mM L-lactate and PEG 3350 (form III).

Surprisingly, crystal form II also appeared to have a ligand bound in the active site. The electron density feature, however, suggested a ligand smaller than L-lactate (Figure 5B). Comparison of the electron density maps for forms I−III clearly showed that the ligand in crystal form II lacked the hydroxyl and methyl groups of L-lactate, yet it appeared to have a carboxyl moiety, based on the strong interaction with Arg555, Arg556, and Lys329 (Figure 5A−C). Thus, an acetate ion was modeled into the density. The average *B*-value for acetate refined to 30 Å^2, which is close to the average *B*-value of the protein (29 Å^2) and comparable to the *B*-values of inhibitors in forms I, III, and IV (25−29 Å^2; see Table 1).

The discovery of an acetate ion bound to the active site prompted us to examine whether acetate is a competitive inhibitor of PutA86−669. Lineweaver−Burk analysis of steady-state inhibition kinetic measurements resulted in a set of lines intersecting at a common *y*-intercept but having different slopes, which is consistent with simple competitive inhibition. The inhibition constant, K_i, was estimated from these data to be 30 mM. Thus, the kinetic data support the modeling of acetate in the active site.

Acetate, L-lactate, and L-THFA bind at the *si* face of the cofactor, surrounded by the FAD, Arg555, Arg556, Lys329, Tyr437, Leu513, Tyr540, Tyr552, Asp370, and Ala436

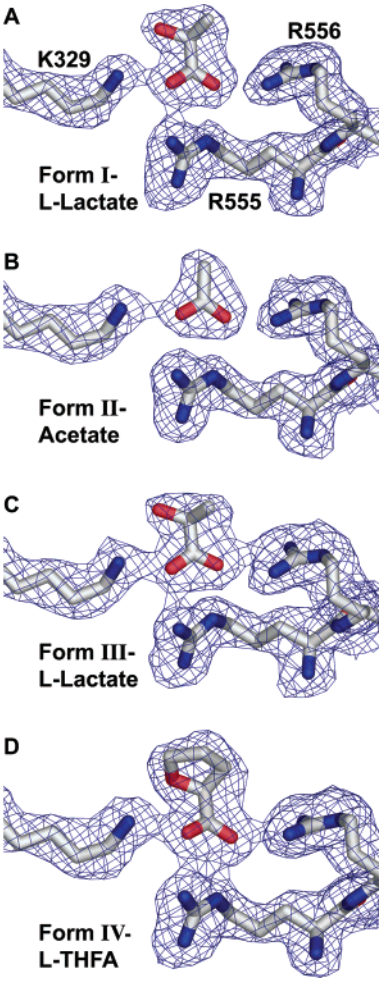

FIGURE 5: Views of the active sites of the four structures showing bound inhibitors interacting with Arg555, Arg556, and Lys329. Panels A−D correspond to crystal forms I−IV, respectively (see Table 1). The electron density maps are simulated annealing $F_o - F_c$ omit maps contoured at 2.5σ.

(Figure 6). The active site conformations of the three complexes are almost identical except for an enlargement of the active site required to accommodate the larger THFA ligand. This increase in active site volume is achieved, in part, by the side chain of Tyr540 flexing upward by 0.5 Å.

The fact that acetate is a competitive inhibitor suggests that the carboxyl moiety is the minimum recognition unit of the PutA PRODH active site. Indeed, the carboxyl groups of all three inhibitors form ion pairs to Arg555, Arg556, and Lys329 (Figure 5). The importance of these ionic interactions is underscored by the nearly universal conservation of these residues in bacterial PutA proteins and eukaryotic PRODH enzymes.

L-Lactate and L-THFA form additional noncovalent interactions with the protein that are absent in the acetate complex, which explains why these molecules are better inhibitors than acetate. For example, both inhibitors hydrogen bond to Tyr437 via a buried active site water molecule (see Figure 6 and ref *27*). The active site water molecule is also present in the acetate complex, but it does not hydrogen bond to the acetate ion. Lys329 (NZ) clearly hydrogen bonds to the lactate hydroxyl (3.2 Å), but the analogous interaction of Lys329 with the L-THFA heteroatom O is weaker (3.5 Å).

Nonpolar interactions are also important for inhibition by L-lactate and L-THFA. The methyl group of L-lactate and

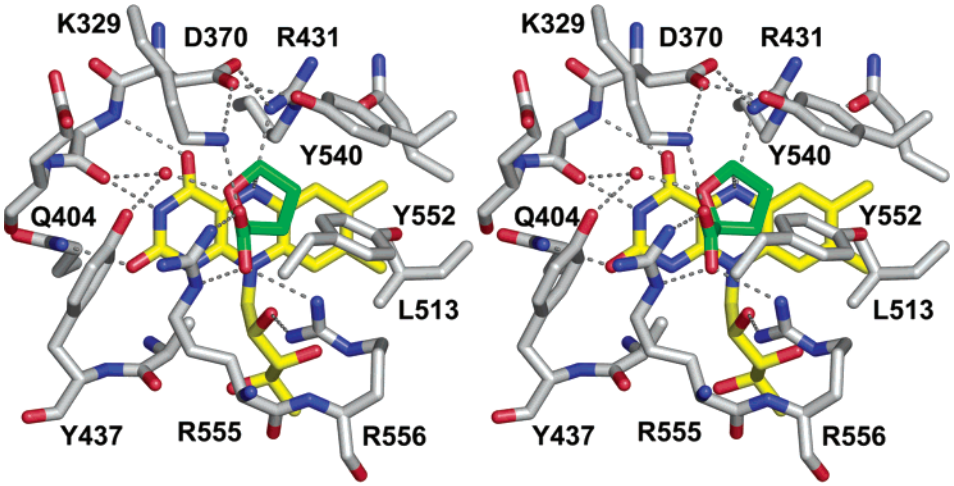

FIGURE 6: Stereoscopic view depicting the active site of the PutA86−669/L-THFA complex (crystal form IV). The dashed lines indicate hydrogen bonds and ion pairs. The dashed line connecting C5 of THFA and N5 of FAD indicates a distance of 3.3 Å. The protein is shown in white, FAD in yellow, and L-THFA in green.

the methylene groups of the L-THFA ring pack tightly against the side chains of Leu513, Tyr540, and Tyr552 (see Figure 6 and ref *27*). These nonpolar interactions could account for the observation that L-THFA is a significantly better inhibitor than L-lactate. L-THFA buries 164 Å^2 of nonpolar surface area in its complex with the enzyme, whereas L-lactate buries only 104 Å^2.

All three inhibitors are completely buried in the protein (ASA = 0 Å^2), which suggests that the substrate is shielded from bulk solvent during catalysis. Burial of the substrate implies that the protein must exhibit flexibility to allow entry and exit of substrates and products. Side chain dihedral rotations could be utilized for this purpose. Most of the side chains in the active site are buried and/or in close contact with other side chains, and their rotation would be severely hindered. On the other hand, Tyr437 forms no hydrogen bonds to the protein, and it separates the active site from bulk solvent. Rotation around χ_1 moves the phenol group of Tyr437 out of the active site and into bulk solvent, exposing a hole that could allow access to the active site. Thus, it is possible that Tyr437 functions as a gate to the active site, although this is somewhat speculative at this time.

L432P Mutation. This mutation was inspired by the discovery of several single-nucleotide polymorphisms (SNPs) in the human *PRODH2* gene possibly linked to schizophrenia susceptibility (*6*). One of these SNPs leads to the L441P mutation of the human protein. This mutation is interesting because it occurs in a region of high amino acid sequence conservation in eukaryotic PRODHs and bacterial PutA proteins and, thus, could greatly impact function.

Human PRODH2 (600 amino acid residues) and the *E. coli* PutA PRODH domain share only 20% amino acid sequence identity, but residues found in the PutA PRODH active site are quite conserved. In fact, of the 40 residues within 5 Å of FAD or lactate/THFA, 19 are identical in the human PRODH2 sequence, and 6 residues display conservative substitutions. Such extensive conservation (47% identity, 62% similarity) argues that the *E. coli* PutA PRODH domain and human PRODH2 share a common active site and possibly a common fold.

The L441P polymorphism in human PRODH was mimicked in PutA86−669 by introducing the homologous

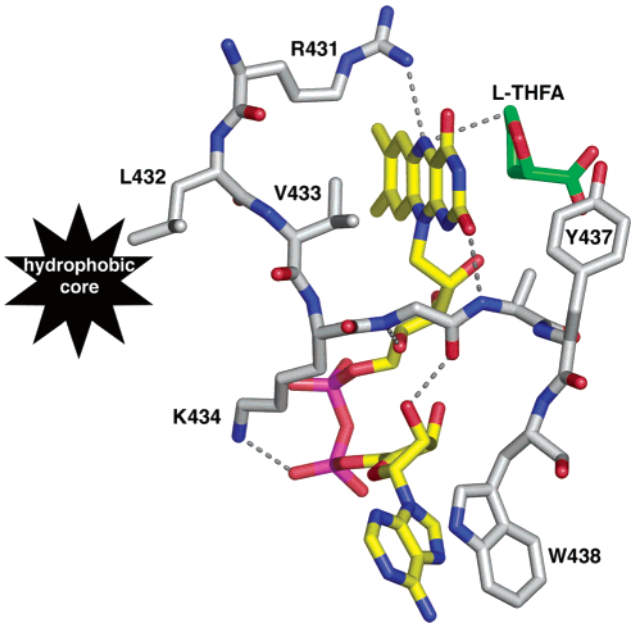

FIGURE 7: Structural context of the L432P mutation of PutA86−669. Residues 431−433 are part of β5, while residues 437−438 are part of α5a. The protein is shown in white, FAD in yellow, and L-THFA in green.

mutation L432P. Note that the approach of mutating a bacterial homologue to study clinically significant human polymorphisms has been used in MTHFR (*43*). Leu432 of PutA resides in the active site near the FAD isoalloxazine (Figure 7). It is located in a highly conserved region of β-strand 5 that supports the *re* face of the FAD. The side chain of Leu432 points away from the FAD into the tightly packed hydrophobic core of the barrel consisting of Ile403, Ala405, Ile414, Ile430, Tyr466, Ala470, Leu473, and Phe484. The main chain of Leu432 is directed toward the *re* face of the FAD. The residues immediately adjacent to Leu432 (Arg431 and Val433) appear to be critical for catalysis and binding FAD. Arg431 (Lys440 in human PRODH2) hydrogen bonds to the FAD N5 (Figure 7). Val433 (Val442 in human PRODH2) directly contacts the FAD through van der Waals interactions (Figure 7).

The mutation resulted in a protein with significantly lower activity and stability. Lineweaver−Burk analysis was used

Table 2: Kinetic Parameters for PutA86−669 and L432P[a]

	K_m (M)	V_{max} (units/mg)	k_{cat} (s^{-1})	k_{cat}/K_m (s^{-1} M^{-1})
PutA86−669 (wild type)	0.060	15.3	17.0	283
L432P	0.13	2.7	3.0	24

[a] Enzyme activity assays were performed at 25 °C using the procedure described previously (*12*, *13*, *28*, *30*).

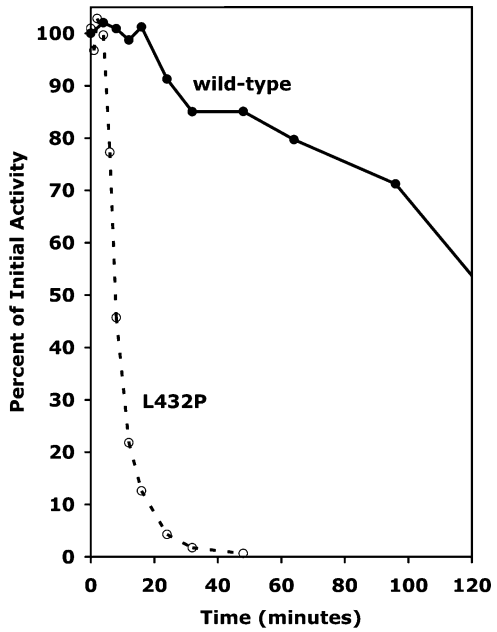

FIGURE 8: Thermostability analysis for wild-type PutA86−669 and L432P at 45 °C. The filled circles and solid curve correspond to data for the wild-type enzyme. The open circles and dashed curve represent data for L432P.

to estimate kinetic parameters for proline of wild-type Puta86−669 and L432P. The kinetic parameters for wild-type PutA86−669 were $K_m = 0.06$ M and $k_{cat} = 17.0$ s^{-1} (Table 2), which are very close to the published values for PutA669 ($K_m = 0.1$ M, $k_{cat} = 16$ s^{-1}) (*28*) and PutA86−601 ($K_m = 0.06$ M, $k_{cat} = 20$ s^{-1}) (*40*). The kinetic parameters for L432P were $K_m = 0.13$ M and $k_{cat} = 3.0$ s^{-1}. Thus, the mutation caused a 5-fold decrease in k_{cat} but had negligible effect on K_m. The L432P mutant enzyme also exhibited significantly decreased thermostability, as evidenced by a plot of specific activity versus time (Figure 8). The wild-type enzyme retained 80% of its initial activity after a 1 h incubation at 45 °C, and a 50% drop in activity was observed after about 2 h. In contrast, L432P lost 50% of its initial activity after only 8 min at 45 °C, and it was completely inactivated in 1 h.

DISCUSSION

Recurrent Features of Flavoenzyme Active Sites. Fraaije and Mattevi analyzed several flavoenzyme structures and found that flavoenzyme dehydrogenases share two common structural features of protein−flavin hydrogen bonding (*45*). The PutA86−669 structures demonstrate that PutA shares these conserved attributes.

First, flavoenzymes typically provide hydrogen partners for the N1−C2═O2 locus of the FAD. These interactions are thought to stabilize the anionic form of the reduced flavin. In the PutA PRODH structures, Gln404 and Ala436 provide these interactions (Figure 4).

Second, there is usually a hydrogen bond donor (typically Arg or Lys) within hydrogen-bonding distance of the flavin N5. This interaction helps to tune the flavin redox potential, probably through two compensating mechanisms corresponding to N5 being a hydrogen bond acceptor when the flavin is oxidized and a donor when the flavin is reduced. Arg431 plays this critical role in PutA (Figures 4, 6, and 7). The distance between N5 and the NH1 atom of Arg431 is 3.1−3.2 Å in the four structures, and the N10−N5−NH1 angle is 160−164°. These values are within those typically found in flavoenzymes (*45*). Arg431 is located on the FAD face opposite to the substrate, which is also a conserved feature of flavoenzyme active site architecture.

Substrate Recognition and Catalytic Mechanism. The structures of the PRODH domain complexed with three different ligands provide insights into the roles of active site residues in substrate recognition. Proline has three functional groups that must be recognized by the enzyme: carboxyl, amine, and methylene groups of the ring (C3−C5). The fact that acetate binds the active site attests to the importance of ionic interactions with the carboxylate. Arg555, Arg556, and Lys329 provide these essential interactions (Figure 5). The heteroatom oxygen of L-THFA in our structure represents the substrate amine group. This atom forms a water-mediated hydrogen bond to Tyr437 (2.6 Å), while interacting with Lys329 (NZ) at a distance of 3.5 Å. The methylene groups of THFA contact Leu513, Tyr540, and Tyr552, which suggests that these residues play the role of enforcing substrate shape and size specificity. They also provide critical nonpolar surface area that helps to bury the methylene groups of the five-membered ring. These interactions must be quite important, since they result in a 6-fold decrease in K_i of THFA compared to L-lactate.

THFA is isostructural to Pro, and thus the PutA86−669/L-THFA structure provides a reasonable view of the E−S complex. The THFA ring is nearly parallel to the flavin tricyclic ring system and centered over the middle ring (Figure 6). The distance between C5 of THFA and the FAD N5 is 3.3 Å, and the N10−N5−C5 angle is 110°. These geometric parameters, which describe the arrangement of the reactive parts of the substrate and flavin, are within the ranges observed for other flavin-dependent dehydrogenases (3.0−3.8 Å, 96−117°) (*45*).

Enzymes provide functional groups that assist substrate activation. There are two aspects of substrate activation to consider for the PRODH reaction. First, the enzyme could provide a base that abstracts a proton from proline C5, producing a carbanion. A potential candidate for this role is Asp370, which is 3.3 Å from the THFA C5. However, mutagenesis and structural data argue strongly against this idea. Mutation of Asp370 to Ala produces no change in K_m and only a 2-fold decrease in k_{cat} (*40*). One would expect a much larger decrease in activity if Asp370 played the role of catalytic base in a carbanion mechanism. Moreover, the geometry of THFA C5 relative to FAD N5 is consistent with direct hydride transfer (*45*). Thus, direct hydride transfer seems to be the most plausible mechanism based on the currently available kinetic and structural data.

A second aspect of substrate activation is deprotonation of the proline amine group, assuming zwitterionic proline binds the active site. The THFA complex suggests that the closest neighbor of the proline amine group is a water

molecule bound to Tyr437. It is therefore possible that the water molecule and Tyr437 play a role in deprotonation of the substrate amine group. Lys329 may assist in this process. Its ammonium group is 3.5 Å from the THFA oxygen heteroatom, which is a favorable interaction. In the E−S complex, however, there would be a repulsive interaction between Lys329 and the positive charge on the amine group of zwitterionic proline, which would favor deprotonation of the substrate. Deprotonation of the substrate amine creates a lone pair on the nitrogen, which can accept a hydrogen bond from Lys329, thus changing a repulsive interaction with Lys329 into an attractive one. The hypothesized effect of Lys329 on the protonation state of the substrate could be significant in the solvent-protected active site, where electrostatic interactions are enhanced. Thus, Lys329 along with Tyr437 probably plays dual roles by helping to stabilize the substrate and product, as well as encouraging deprotonation of the substrate amine group.

L432P Mutation. This active site mutation caused a 10-fold decrease in k_{cat}/K_m (primarily due to a 5-fold decrease in k_{cat}) and a severe loss in thermostability. The unchanged K_m for proline is consistent with the fact that Leu432 does not contact the inhibitors in our structures. The 5-fold decrease in k_{cat} suggests that proline and FAD are not aligned optimally for catalysis in L432P, due presumably to a disruption of FAD−protein interactions. This interpretation is consistent with the location of Leu432 between two residues that directly contact FAD. The introduction of Pro at position 432 presumably alters the local polypeptide conformation, which would likely disrupt important protein−FAD interactions provided by the adjacent residues Arg431 and Val433. The loss in activity observed in the L432P mutant was most likely due, in part, to a disruption of the important Arg431−N5 interaction. The decrease in thermostability for L432P is consistent with the location of Leu432 in the hydrophobic core. The mutation to proline almost certainly alters the tight packing within the hydrophobic core, possibly creating a cavity. It is known that mutations that cause repacking of the hydrophobic core almost invariably reduce stability (*46*). Thus, the results from our work on the PutA86−669 L432P mutant suggest that the molecular basis for increased plasma proline levels in schizophrenic subjects carrying the missense mutation L441P is due to decreased stability of PRODH2 (*8*).

Conformational Changes Caused by Inhibitor Binding. An intriguing aspect of PutA structure and function is the mechanism by which the protein switches between its repressor and enzymatic roles. It is thought that reduction of the FAD induces conformational changes that cause PutA to switch from being a DNA-bound repressor to a membrane-associated bifunctional enzyme. Zhu and Becker have used limited proteolysis to examine the structural changes in full-length PutA caused by flavin reduction and inhibitor binding (*47*). Their work suggests that there are at least three conformations of PutA corresponding to (1) oxidized FAD with no ligand in the PRODH active site, (2) oxidized FAD with a ligand in the PRODH active site, and (3) reduced FAD. The structures presented here represent conformation 2. Work is ongoing to obtain crystal forms of PutA conformations 1 and 3. The structure of conformation 1 has remained elusive because of the apparent affinity of the PRODH active site for small carboxylate-containing ligands and the presence of such ligands in commercially available PEG.

ACKNOWLEDGMENT

We thank Beverly DaGue of the University of Missouri−Columbia Proteomics Center for help with mass spectroscopy analysis of crystals. We also thank the personnel of APS beamline 19-ID for assistance with data collection, especially Stephan L. Ginell, Younchang Kim, Frank Rotella, and Jack Lazarz. Use of the Argonne National Laboratory Structural Biology Center beamlines at the Advanced Photon Source was supported by the U.S. Department of Energy, Office of Energy Research, under Contract W-31-109-ENG-38.

REFERENCES

1. Phang, J. M. (1985) The regulatory functions of proline and pyrroline-5-carboxylic acid, *Curr. Top. Cell Regul. 25*, 92−132.
2. Adams, E., and Frank, L. (1980) Metabolism of proline and the hydroxyprolines, *Annu. Rev. Biochem. 49*, 1005−1061.
3. Donald, S. P., Sun, X. Y., Hu, C. A., Yu, J., Mei, J. M., Valle, D., and Phang, J. M. (2001) Proline oxidase, encoded by p53-induced gene-6, catalyzes the generation of proline-dependent reactive oxygen species, *Cancer Res. 61*, 1810−1815.
4. Polyak, K., Xia, Y., Zweier, J. L., Kinzler, K. W., and Vogelstein, B. (1997) A model for p53-induced apoptosis, *Nature 389*, 300−305.
5. Maxwell, S. A., and Davis, G. E. (2000) Differential gene expression in p53-mediated apoptosis-resistant vs. apoptosis-sensitive tumor cell lines, *Proc. Natl. Acad. Sci. U.S.A. 97*, 13009−13014.
6. Liu, H., Heath, S. C., Sobin, C., Roos, J. L., Galke, B. L., Blundell, M. L., Lenane, M., Robertson, B., Wijsman, E. M., Rapoport, J. L., Gogos, J. A., and Karayiorgou, M. (2002) Genetic variation at the 22q11 PRODH2/DGCR6 locus presents an unusual pattern and increases susceptibility to schizophrenia, *Proc. Natl. Acad. Sci. U.S.A. 99*, 3717−3722.
7. Liu, H., Abecasis, G. R., Heath, S. C., Knowles, A., Demars, S., Chen, Y. J., Roos, J. L., Rapoport, J. L., Gogos, J. A., and Karayiorgou, M. (2002) Genetic variation in the 22q11 locus and susceptibility to schizophrenia, *Proc. Natl. Acad. Sci. U.S.A. 99*, 16859−16864.
8. Jacquet, H., Raux, G., Thibaut, F., Hecketsweiler, B., Houy, E., Demilly, C., Haouzir, S., Allio, G., Fouldrin, G., Drouin, V., Bou, J., Petit, M., Campion, D., and Frebourg, T. (2002) PRODH mutations and hyperprolinemia in a subset of schizophrenic patients, *Hum. Mol. Genet. 11*, 2243−2249.
9. Williams, H. J., Williams, N., Spurlock, G., Norton, N., Zammit, S., Kirov, G., Owen, M. J., and O'Donovan, M. C. (2003) Detailed analysis of PRODH and PsPRODH reveals no association with schizophrenia, *Am. J. Med. Genet. 120B*, 42−46.
10. Harrison, P. J., and Owen, M. J. (2003) Genes for schizophrenia? Recent findings and their pathophysiological implications, *Lancet 361*, 417−419.
11. Karayiorgou, M., and Gogos, J. A. (2003) Genes for schizophrenia, *Lancet 361*, 1828−1829; author reply 1829−1830.
12. Brown, E. D., and Wood, J. M. (1993) Conformational change and membrane association of the PutA protein are coincident with reduction of its FAD cofactor by proline, *J. Biol. Chem. 268*, 8972−8979.
13. Brown, E., and Wood, J. M. (1992) Redesigned purification yields a fully functional PutA protein dimer from *Escherichia coli*, *J. Biol. Chem. 267*, 13086−13092.
14. Becker, D. F., and Thomas, E. A. (2001) Redox properties of the PutA protein from *Escherichia coli* and the influence of the flavin redox state on PutA-DNA interactions, *Biochemistry 40*, 4714−4722.
15. Menzel, R., and Roth, J. (1981) Purification of the *put*A gene product, *J. Biol. Chem. 256*, 9755−9761.
16. Menzel, R., and Roth, J. (1981) Enzymatic properties of the purified *putA* protein from *Salmonella typhimurium*, *J. Biol. Chem. 256*, 9762−9766.
17. Surber, M. W., and Maloy, S. (1999) Regulation of flavin dehydrogenase compartmentalization: Requirements for PutA-

membrane association in *Salmonella typhimurium*, *Biochim. Biophys. Acta 1421*, 5−18.
18. Wood, J. (1987) Membrane association of proline dehydrogenase in *Escherichia coli* is redox dependent, *Proc. Natl. Acad. Sci. U.S.A. 84*, 373−377.
19. Menzel, R., and Roth, J. (1981) Regulation of genes for proline utilization in *Salmonella typhimurium*: Autogenous repression by the *putA* gene product, *J. Mol. Biol. 148*, 21−44.
20. Ostrovsky De Spicer, P., and Maloy, S. (1993) PutA protein, a membrane-associated flavin dehydrogenase, acts as a redox-dependent transcriptional regulator, *Proc. Natl. Acad. Sci. U.S.A. 90*, 4295−4298.
21. Wood, J. M. (1981) Genetics of L-proline utilization in *Eschericia coli*, *J. Bacteriol. 146*, 895−901.
22. Gu, D., Zhou, Y., Kallhoff, V., Baban, B., Tanner, J. J., and Becker, D. F. (2004) Identification and characterization of the DNA-binding domain of the multifunctional PutA flavoenzyme, *J. Biol. Chem. 279*, 31171−31176.
23. Tritsch, D., Mawlawi, H., and Biellmann, J. F. (1993) Mechanism-based inhibition of proline dehydrogenase by proline analogues, *Biochim. Biophys. Acta 1202*, 77−81.
24. Kowaloff, E. M., Phang, J. M., Granger, A. S., and Downing, S. J. (1977) Regulation of proline oxidase activity by lactate, *Proc. Natl. Acad. Sci. U.S.A. 74*, 5368−5371.
25. Scarpulla, R. C., and Soffer, R. L. (1978) Membrane-bound proline dehydrogenase from *Escherichia coli*, *J. Biol. Chem. 253*, 5997−6001.
26. Zhu, W., Gincherman, Y., Docherty, P., Spilling, C. D., and Becker, D. F. (2002) Effects of proline analog binding on the spectroscopic and redox properties of PutA, *Arch. Biochem. Biophys. 408*, 131−136.
27. Lee, Y. H., Nadaraia, S., Gu, D., Becker, D. F., and Tanner, J. J. (2003) Structure of the proline dehydrogenase domain of the multifunctional PutA flavoprotein, *Nat. Struct. Biol. 10*, 109−114.
28. Vinod, M. P., Bellur, P., and Becker, D. F. (2002) Electrochemical and functional characterization of the proline dehydrogenase domain of the PutA flavoprotein from *Escherichia coli*, *Biochemistry 41*, 6525−6532.
29. Nadaraia, S., Lee, Y. H., Becker, D. F., and Tanner, J. J. (2001) Crystallization and preliminary crystallographic analysis of the proline dehydrogenase domain of the multifunctional PutA flavoprotein from *Escherichia coli*, *Acta Crystallogr. D57*, 1925−1927.
30. Abrahamson, J. L. A., Baker, L. G., Stephenson, J. T., and Wood, J. M. (1983) Proline dehydrogenase from *Escherichia* K12, properties of the membrane-associated enzyme, *Eur. J. Biochem. 134*, 77−82.
31. Zhang, M., and Tanner, J. J. (2004) Detection of L-lactate in poly(ethylene glycol) solutions confirms the identity of the active-site ligand in a proline dehydrogenase structure, *Acta Crystallogr. D60*, 985−986.
32. Otwinowski, Z., and Minor, W. (1997) Processing of X-ray diffraction data collected in oscillation mode, *Methods Enzymol. 276*, 307−326.
33. Matthews, B. W. (1968) Solvent content of protein crystals, *J. Mol. Biol. 33*, 491−497.
34. Brünger, A. T., Adams, P. D., Clore, G. M., DeLano, W. L., Gros, P., Grosse-Kunstleve, R. W., Jiang, J. S., Kuszewski, J., Nilges, M., Pannu, N. S., Read, R. J., Rice, L. M., Simonson, T., and Warren, G. L. (1998) Crystallography & NMR system: A new software suite for macromolecular structure determination, *Acta Crystallogr. D54*, 905−921.
35. Winn, M. D., Isupov, M. N., and Murshudov, G. N. (2001) Use of TLS parameters to model anisotropic displacements in macromolecular refinement, *Acta Crystallogr. D57*, 122−133.
36. Project, C. C. (1994) The CCP4 suite: Programs for protein crystallography, *Acta Crystallogr. D50*, 760−763.
37. van Aalten, D. M., Bywater, R., Findlay, J. B., Hendlich, M., Hooft, R. W., and Vriend, G. (1996) PRODRG, a program for generating molecular topologies and unique molecular descriptors from coordinates of small molecules, *J. Comput.-Aided Mol. Des. 10*, 255−262.
38. DeLano, W. L. (2002) The PyMOL Molecular Graphics System (http://www.pymol.org).
39. Sobolev, V., Sorokine, A., Prilusky, J., Abola, E. E., and Edelman, M. (1999) Automated analysis of interatomic contacts in proteins, *Bioinformatics 15*, 327−332.
40. Baban, B. A., Vinod, M. P., Tanner, J. J., and Becker, D. F. (2004) Probing a hydrogen bond pair and the FAD redox properties in the proline dehydrogenase domain of *Escherichia coli* PutA, *Biochim. Biophys. Acta 1701*, 49−59.
41. Rehmann, H., Prakash, B., Wolf, E., Rueppel, A., De Rooij, J., Bos, J. L., and Wittinghofer, A. (2003) Structure and regulation of the cAMP-binding domains of Epac2, *Nat. Struct. Biol. 10*, 26−32.
42. Andreeva, A., Howorth, D., Brenner, S. E., Hubbard, T. J., Chothia, C., and Murzin, A. G. (2004) SCOP database in 2004: refinements integrate structure and sequence family data, *Nucleic Acids Res. 32* (database issue, D226−D229).
43. Guenther, B. D., Sheppard, C. A., Tran, P., Rozen, R., Matthews, R. G., and Ludwig, M. L. (1999) The structure and properties of methylenetetrahydrofolate reductase from *Escherichia coli* suggest how folate ameliorates human hyperhomocysteinemia, *Nat. Struct. Biol. 6*, 359−365.
44. Krissinel, E., and Henrick, K. (2003) Protein structure comparison in 3D based on secondary structure matching (SSM) followed by Ca alignment, scored by a new structural similarity function, *Int. Conf. Mol. Struct. Biol., 5th*, 88.
45. Fraaije, M. W., and Mattevi, A. (2000) Flavoenzymes: diverse catalysts with recurrent features, *Trends Biochem. Sci. 25*, 126−132.
46. Mooers, B. H., Datta, D., Baase, W. A., Zollars, E. S., Mayo, S. L., and Matthews, B. W. (2003) Repacking the core of T4 lysozyme by automated design, *J. Mol. Biol. 332*, 741−756.
47. Zhu, W., and Becker, D. F. (2003) Flavin redox state triggers conformational changes in the PutA protein from *Escherichia coli*, *Biochemistry 42*, 5469−5477.
48. Engh, R. A., and Huber, R. (1991) Accurate bond and angle parameters for X-ray protein structure refinement, *Acta Crystallogr. A47*, 392−400.
49. Laskowski, R. A., MacArthur, M. W., Moss, D. S., and Thornton, J. M. (1993) PROCHECK: a program to check the stereochemical quality of protein structures, *J. Appl. Crystallogr. 26*, 283−291.
50. Shindyalov, I. N., and Bourne, P. E. (1998) Protein structure alignment by incremental combinatorial extension (CE) of the optimal path, *Protein Eng. 11*, 739−747.

BI048737E